Nonlinear temporal dynamics in multifunctional nanoantenna with asymmetry

YE ZHANG, XINCHEN JIANG, 2,3,5 D ANDREY NOVITSKY, 3,4 D AND LEI GAO 1,2,3,6

Abstract: A new concept of a nonlinear nanoantenna with multiple functions is suggested. We give theoretical research on the temporal dynamics for this asymmetric system which consistis of a pair of graphene-wrapped dielectric nanoparticles with tunable Fermi energies. It is demonstrated that asymmetry can lead to an enlarged stationary multistable regime and enrich the temporal dynamical behaviors compared to the symmetry counterpart. Such a nanoantenna can provide a chance to switch among coexisting nonlinear states under the illumination of a sequence of external pulses, which simultaneously leads to not only the manipulation of the angular scanning sector and scattering pattern of nanoantenna but also the controllable multistate optical switching or coding element. This kind of asymmetric dimer system may represent a possible step toward the development of tunable applications in nonlinear nanophotonics and biophotonics.

© 2025 Optica Publishing Group under the terms of the Optica Open Access Publishing Agreement

1. Introduction

With the great development of nanotechnology, the research on optics at nanoscale has become a hot and frontier topic. Most previous studies of nanophotonic were predominantly focused on the linear system however nonlinear effects lead to richer phenomena [1,2]. Nonlinear optics has important applications in modern optical devices such as ultrafast optical switch [3,4], active all-optical control [5] and fiber sensor [6]. Except for the stationary research of the system, the study of temporal dynamics focuses on the dynamic behavior of the system on time scales, in particular showing novel properties under the influence of nonlinear effects [7]. In view of the above, it is able to create large-scale photonic integrated circuits [8], realizing elaboration of micro- and nanostructures [9] and generating coherent electromagnetic waves through nonlinear parametric processes [10–12]. In addition, due to the complex dynamic features of chaos, it has remarkable application in random bit generator [13,14], Chua's oscillator circuit [15] and multimode lasers [16].

The study of nonlinear temporal dynamics is important for understanding and controlling the nature and behavior of systems, and how to obtain more intense and faster nonlinear effects has been a hot research topic. One of the important ways is to enhance and control the nonlinear optical response utilizing plasmons, and the research results are numerous. For nanoparticle systems, a nanoantenna made of two identical nonlinear metallic nanoparticles can achieve periodic scanning of the scattering pattern [17,18], the routes to chaos in nanostructures can be of

#562188 Journal © 2025

¹School of Physical Science and Technology, Soochow University, Suzhou 215006, China & Collaborative Innovation Center of Suzhou Nano Science and Technology & Jiangsu Key Laboratory of Frontier Materia Physics and Devices, Soochow University, Suzhou 215006, China

²School of Optical and Electronic Information, Suzhou City University, Suzhou 215104, China

³Jiangsu Key Laboratory of Biophotonics & Suzhou Key Laboratory of Biophotonics & SZCU-ITU International Joint MetaCenter for Advanced Photonics and Electronics, Suzhou City University, Suzhou 215104, China

⁴Depertment of Physical Optics and Applied Informatics, Belarusian State University, Minsk 220030, Belarus

⁵xcjiang@szcu.edu.cn

⁶leigao@suda.edu.cn

great insight into nanophotonics [19] and the system of linear and nonlinear combinations enables ultrafast encryption through switching between the forward and backward directions [20,21]. In more complex nonlinear plasmonic nanostructures, such as nanocomposite materials [22], nanoparticle arrays [23,24] and chain structures [25,26], nonlinear dynamics are abundant owing to well periodicity and flexibility. In addition, due to the complex behaviors at nanoscale, both theoretical models and experimental techniques need to be further investigated and developed. Recently, some scholars have considered the influence of nonlocal effects on the nonlinear structure [27,28]. With the continuous development of two-dimensional materials, graphene becomes a promising alternative to traditional materials such as metals and other plasmonic materials, because it can not only support plasmons in a wide spectral range from the terahertz (THz) to the visible frequencies, but also has more intense nonlinear response [29]. Research finds that composite systems composed of graphene and other materials can act as nonlinear nanophotonic circuitry [30], modulate the switching thresholds of bistability [31,32] and form optical multistability [33,34]. Recently it has also been considered how the asymmetry of the structure affects the optical response of the nanodimer made of a pair of graphene-wrapped dielectric [35,36]. However, traditional methods rely on structural engineering to generate asymmetry, and once the structure is fixed, the asymmetry cannot be adjusted. Yet, no attention has been paid to modulating the asymmetry of the system through Fermi energy of graphene. Practically, the Fermi energy of the graphene layer can be electrically controlled by utilizing a gate voltage without changing the micro-architecture, and the graphene-wrapped nanoparticles can be produced by layer-by-layer self-assembly or precursor-assisted chemical vapor deposition [37,38]. This approach significantly enhances the tenability of system, eliminates the need for complex nanofabrication, and enables adaptability to diverse working environments.

In this paper, we explore a comprehensive theoretical and numerical analysis of the nonlinear temporal dynamics exhibited by an asymmetric nanoantenna composed of a pair of graphene-wrapped dielectric nanoparticles with tunable Fermi energies. As a proof of principle, we map the distribution of stable and unstable states in the stationary case and conduct an in-depth investigation of the corresponding temporal dynamical behavior. Moreover, we introduce pulse sequences to enable switching between coexisting states, paving the way for tunable and multifunctional nanodevices.

2. Theoretical model

A plane wave with the frequency ω in the vicinity of the resonant frequency of plasmonic nanoparticles illuminates the nanodimer with radii a and center-to-center spacing d embedded in host medium ($\varepsilon_h = 1$), as shown in Fig. 1. The nanodimer system consists of a pair of asymmetrical nanoparticles which are BaF₂ dielectric spheres ($\varepsilon_{1,2} = 2$) [39] wrapped with graphene layers with different parameters. The radius of the dielectric particle is much larger than the thickness of graphene, so the graphene layers can be characterized well as a 2D film with Kerr-nonlinearity, which can be described as $\sigma = \sigma_L + \sigma_{NL}|E_{in}|^2$. Here, σ_L and σ_{NL} indicate the linear and Kerr-nonlinear parts of the conductivity respectively, and E_{in} is the local electric field inside the graphene layer. Moreover, the linear term can be generally described in Drude-like form at room temperature. Thus, we get [40,41]

$$\sigma_L^n = \frac{ie^2}{\pi \hbar^2} \frac{E_{Fn}}{(\omega + i\xi^{-1})}, \sigma_{NL}^n = -i\frac{9}{8} \frac{e^4}{\pi \hbar^2} \left(\frac{v_F^2}{E_{Fn}\omega^3}\right), \tag{1}$$

where *n* represents the *n*th nanoparticle, *e* is the electron charge, \hbar is reduced Planck constant, ξ and v_F are electron-phonon relaxation time and Fermi velocity taken as $\xi = 0.3$ ps and $v_F \approx c/300$, respectively, and E_{Fn} is the Fermi energy.

In consideration of the long-wavelength approximation, we assume $a/d \le 1/3$ in order to satisfy the point dipole approximation in the terahertz range [42]. Thus, we can start with the

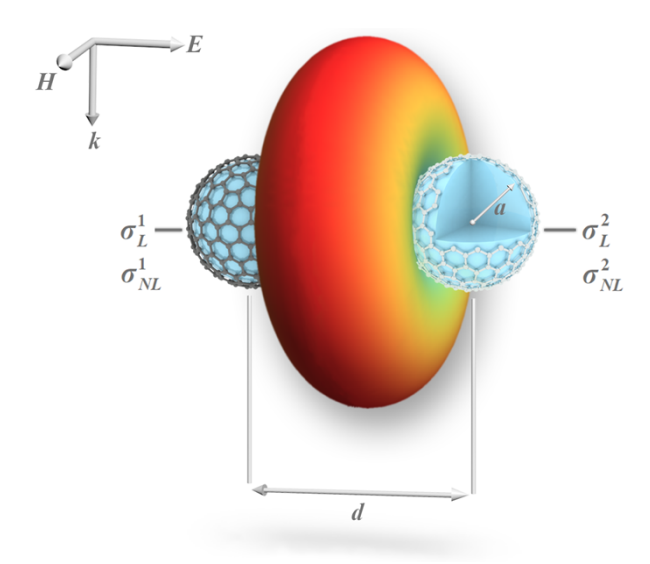


Fig. 1. Schematic of a pair of nanoparticles illuminated by a plane wave with electric field parallel to the dimer axis. The nanoparticles are composed of dielectric spheres wrapped by tunable graphene layers with different Fermi energy, which leads to the asymmetric characterization.

theoretical development of the electric dipole moment p_n (n = 1, 2) as

$$\begin{cases}
\alpha_1^{-1} \mathbf{p}_1 = \mathbf{E}_i + \mathbf{E}_{12} \\
\alpha_2^{-1} \mathbf{p}_2 = \mathbf{E}_i + \mathbf{E}_{21}
\end{cases}$$
(2)

Here, α_n indicates the corresponding electric polarizabilities of the two nanoparticles, $E_i = E_0 e^{i(kz-\omega t)} e_y$ is the incident external field which is polarized along the y axis and propagates along z axis, $E_{12} = (1 - ikd) \frac{2p_2}{\varepsilon_h d^3} e^{ikd}$ ($E_{21} = (1 - ikd) \frac{2p_1}{\varepsilon_h d^3} e^{ikd}$) indicates the dipolar interactions between the two nanoparticles, $k = \sqrt{\varepsilon_h \omega/c}$ is the wave vector. Furthermore, following the spirit of the dispersion relation method [30,43], α_n^{-1} can be decomposed in the vicinity of the resonant frequencies of the nanoparticles, and only keep the first-order terms involving time derivatives in the assumption of weak nonlinearity, dissipation and detuning in this nanodimer system [25,44],

$$\alpha_n^{-1}(\omega) \approx \alpha_n^{-1}(\omega_n) + \left. \frac{d\alpha_n^{-1}}{d\omega} \right|_{\omega = \omega_n} \left(\Delta \omega_n + i \frac{\mathrm{d}}{\mathrm{d}t} \right).$$
 (3)

Here, $\Delta\omega_n = \omega - \omega_n$ is the detuning variable, where ω_n is the dipole resonant frequency of an individual nanoparticle when neglecting the nonlinear and coupling effects:

$$\omega_n = \sqrt{\frac{2e^2 E_{Fn}}{a\varepsilon_0 \pi \hbar^2 (\varepsilon + 2\varepsilon_h)} - \xi^{-2}}.$$
 (4)

By substituting Eqs. (3) and (4) into Eq. (2) and applying dimensionless processing, the dynamical equations of the nonlinear coupled nanodimer system can be derived as

$$\begin{cases}
i \frac{\omega_{1}^{2}}{\omega_{1}^{2} + \xi^{-2}} \frac{dP_{1}}{d\tau} + \left(\frac{\omega_{1}^{2}}{\omega_{1}^{2} + \xi^{-2}} \Omega_{1} + i\gamma_{1} + |P_{1}|^{2}\right) P_{1} + GP_{2} = E \\
i \frac{\omega_{1} \omega_{2}}{\omega_{2}^{2} + \xi^{-2}} \frac{dP_{2}}{d\tau} + \left(\frac{\omega_{2}^{2}}{\omega_{2}^{2} + \xi^{-2}} \Omega_{2} + i\gamma_{2} + v^{2} |P_{2}|^{2}\right) P_{2} + GP_{1} = E
\end{cases}$$
(5)

where τ , Ω_n , γ_n , G, ν , P_n and E indicate the dimensionless time, detuning parameters, thermal and radiation losses, dimensionless coupling coefficient, asymmetry factor, and dimensionless slowly varying amplitudes of the dipole moments and external field, respectively. The detailed expressions of these parameters are given below as

$$\tau = \omega_{1}t, \Omega_{n} = \frac{\omega - \omega_{n}}{\omega_{n}}, \gamma_{n} = \frac{\xi^{-1}}{2\omega_{n}} + \frac{\varepsilon_{h}k^{3}a^{3}}{\varepsilon + 2\varepsilon_{h}},$$

$$G = \frac{3\varepsilon_{h}}{\varepsilon + 2\varepsilon_{h}} \left(\frac{a}{d}\right)^{3} (1 - ikd)e^{ikd}, \nu = \sqrt{\frac{\omega_{1}\sigma_{NL}^{2}(\omega_{2})}{\omega_{2}\sigma_{NL}^{1}(\omega_{1})}},$$

$$P_{n} = \frac{p_{n}}{\varepsilon_{h}a^{3}} \sqrt{\frac{i\sigma_{NL}^{1}(\omega_{1})}{\omega_{1}a\varepsilon_{0}(\varepsilon + 2\varepsilon_{h})}}, E = \frac{-3\varepsilon_{h}E_{0}}{2(\varepsilon + 2\varepsilon_{h})} \sqrt{\frac{i\sigma_{NL}^{1}(\omega_{1})}{\omega_{1}a\varepsilon_{0}(\varepsilon + 2\varepsilon_{h})}}.$$
(6)

Furthermore, one should notice that when the parameters of graphene layers of nanoparticles are identical, the dynamical equations will naturally reduce to a symmetry case [30], i.e., $\omega_1 = \omega_2$, $\Omega_1 = \Omega_2$, $\gamma_1 = \gamma_2$ and $\nu = 1$.

In the framework of Eq. (5), the calculation of stationary solutions constitutes the crucial first step for understanding the states of system. Considering $dP_{1,2}/dt = 0$ in Eq. (5), we can derive the static nonlinear equations and determine that there are nontrivial solutions of the dipole moments in the following parameter space [21,45,46]:

$$\frac{\omega_{1,2}^2 \Omega_{1,2}}{\omega_{1,2}^2 + \xi^{-2}} < -\operatorname{Re}[G] - \sqrt{3}|\gamma_{1,2} - \operatorname{Im}[G]|. \tag{7}$$

Further analysis on these stationary solutions should involve the calculation of the eigenvalues of the corresponding Jacobian matrix of Eq. (5), in order to determine the stability of the static states. Only if all of the real parts of the eigenvalues of Jacobian matrix are negative, a stationary solution can be identified as a stable state whose far-field scattering intensity is time invariant, and unstable states will give rise to new phenomena in subsequent dynamic investigation. Based on the analysis of stationary solutions, we employ the fourth-order Runge-Kutta scheme to numerically research the temporal behaviors of Eq. (5) in detail by considering the variable parameters of the graphene layers and the external fields [19,35].

In addition, we also introduce a dimensionless scattering intensity of the dipole pair to illustrate the far-field optical dynamical behaviors of this nanodimer system at a macroscopic level [30]:

$$U_{s}(\theta, \varphi, \tau) = (1 - \sin^{2}\theta \sin^{2}\varphi)[|P_{1}(\tau)|^{2} + |P_{2}(\tau)|^{2} + 2|P_{1}(\tau)||P_{2}(\tau)|\cos(\Delta\Psi + kd\sin\theta\sin\varphi)]^{2}$$
(8)

where θ and φ are the spherical polar and azimuthal angles, and $\Delta\Psi$ indicates the phase difference between $P_1(\tau)$ and $P_2(\tau)$.

3. Results and discussion

In what follows, we have carried out temporal dynamics analysis based on the proposed theoretical model. The proposed nanodimer system can be viewed as an optical nanoantenna with asymmetry [17,47]. This asymmetry arises from the fact that the graphene layers wrapped on the two dielectric spheres can have different Fermi energy, which leads to the asymmetric characterization of the linear and nonlinear terms. In this work, we consider fixed a = 100 nm, d = 300 nm, $E_{F1} = 0.9$ eV and variable E_{F2} which can modulate the asymmetry of the nanodimer system.

With $\Omega_1 = -0.1$, Fig. 2 presents the nonlinear behaviors in both static and dynamical levels of the asymmetrical nanodimer system for $E_{F2} = 0.85$ eV, which explicitly includes the intensity of the dimensionless dipole moments $|P_{1,2}|$ in microscopic level and typical forward scattering intensity $U_s(\theta = 0, \varphi, \tau)$ in macroscopic level. In order to distinguish the linear stable and

unstable solutions in Fig. 2, we utilize the dark and light colors to present the stable and unstable states respectively. Obviously, one can observe the multistable regime, which can emerge in the vicinity of E=0.015 according to the left panels of Fig. 2. In the meantime, by comparing the values of $|P_{1,2}|$ shown in Fig. 2(a) and 2(b) under the particular E, the symmetry breaking can lead to inconsistency of the dipole moments of the two nanoparticles, which is quite different from the case of symmetrical system [30]. However, the number of stable and unstable solutions for $|P_1|$, $|P_2|$ and U is equal, and regime without stable states corresponds to the background field E ranging from 0.0076 to 0.0089.

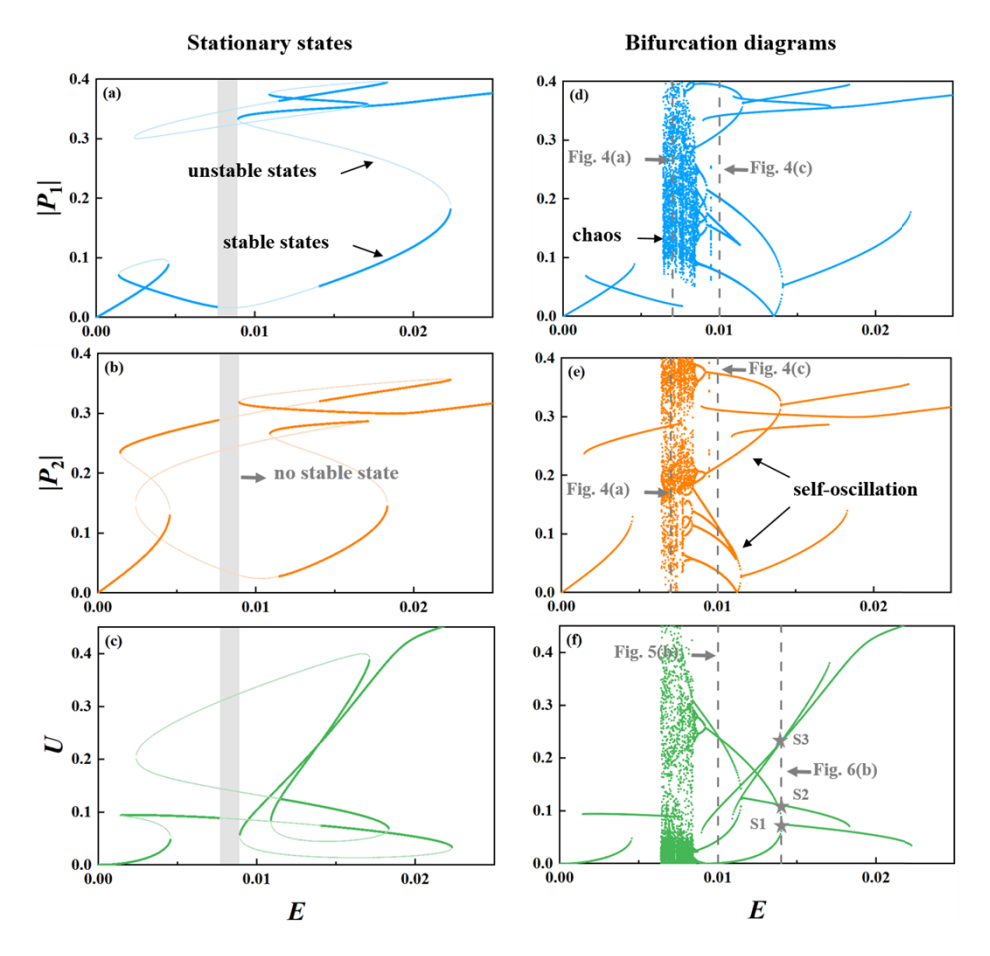


Fig. 2. Characterization of the stationary states and nonlinear dynamics in the asymmetry system with $E_{F1} = 0.9$ eV, $E_{F2} = 0.85$ eV. In the left panels (a-c) show the stationary states for the absolute values of the dimensionless dipole moment $|P_1|$, $|P_2|$ and forward scattering intensity U, dark and light colors mark the corresponding stable and unstable states, and the gray region indicates the regime with no stable state. The right panels (d-f) indicate the corresponding bifurcation diagrams of dynamical analysis. In addition to the stable static states, there appear periodic self-oscillations, period doubling and chaos phenomenon. The background field intensity indicated by gray dashed lines and three stable solutions marked by stars S1,S2,S3 will be further researched later.

To reveal the temporal dynamical behaviors of the linearly unstable solutions in this asymmetric nanodimer system, we numerically simulate the evolutions of the static solutions based on the fourth-order Runge-Kutta scheme. Simultaneously, we record the extrema of $|P_1(\tau)|$, $|P_2(\tau)|$ and

 $U(\tau)$ during the simulation in order to generate the bifurcation diagrams shown in Fig. 2(d-f) by the Poincaré section method. In these diagrams, the linear stable static solutions are consistent with the results shown in the left counterparts, while the nontrivial dynamical solutions or the modulational instabilities can be presented simultaneously. These dynamical solutions involve the periodic self-oscillations, period doubling and chaotic behavior. As shown in Fig. 2(f) at macroscopic level, with the decrease of E from 0.02, we first detect the Hopf bifurcation at 0.014 which is followed by the self-oscillation state. With the further decrease of E, another Hopf bifurcation can emerge at 0.012, and similar self-oscillation state can be detected but with different period. Both of the self-oscillations can undergo a period-doubling bifurcation and develop into a chaotic behavior with the further decrease of E, which is considered as a classical route for the generation of chaos. However, if we in turn increase E from 0, it seems that there is a direct path from stable static state to chaos. In addition, we also find that the stable static states can coexist with the periodic oscillations and the chaos under the same background field. Specifically, two distinct periodic self-oscillations come from the asymmetric characteristics of dipole moments which are absent in the symmetric system [35].

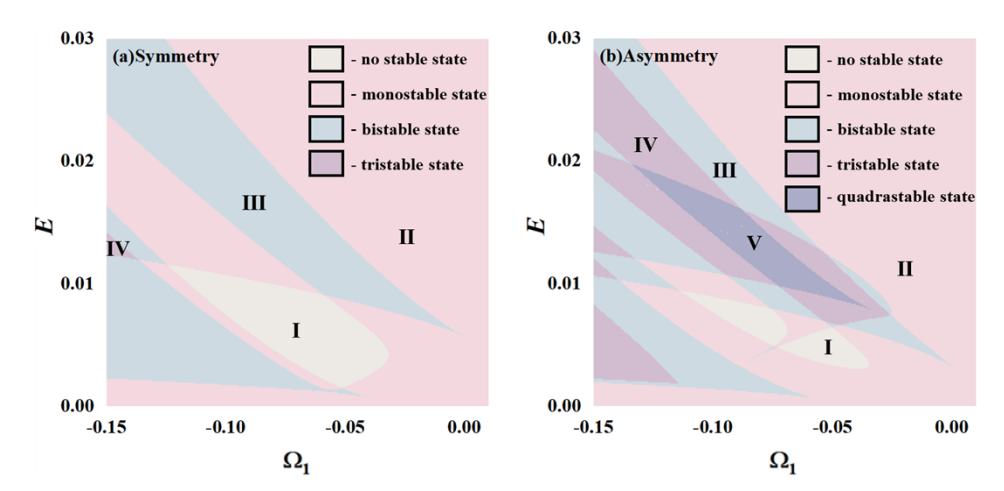


Fig. 3. Distribution of stable static states of the nanodimer system, in the parameters (Ω_1, E) plane. (a) symmetrical case of $E_{F1} = E_{F2} = 0.9$ eV. (b) asymmetric case of $E_{F1} = 0.9$ eV, $E_{F2} = 0.85$ eV. The colors and I, II, III, IV, V denote different regions corresponding to the number of stable states.

In order to reveal the general scenario of the static states in symmetric and asymmetric cases, we present the phase diagrams based on static nonlinear equations for the symmetric and asymmetric cases in the parameters space of (Ω_1, E) . In Fig. 3, we denote the corresponding color regimes (I, II, III, IV, V) into no stable state, monostable state, bistable state, tristable state and quadrastable state respectively. Obviously, the bistable state can be detected in a large range of parameter space, which means that the nanodimer system can present possible switching between two kinds of stable scattering states under the same parameter. Notably, for strong detuning, the symmetric nanodimer also appears as a small regime of tristability, in which the system can have three stable scattering states. In consideration of asymmetry, we can find that the regimes of multistability are enlarged and accompanied with the emergence of quadrastability, as depicted in Fig. 3(b). This phenomenon arises from the nonlinearity of graphene and the inconsistency of the dipole moments of nanoparticles due to asymmetry. In the meantime, we also find that all of the regimes are not contiguous, but are separated into several pieces in the phase diagram, which means that the number of stable static states is highly sensitive to the external field and detuning parameter, i.e., E_{F2} . Hence, the nonlinear behavior can be easily tuned in this dimer system.

To further distinguish the temporal dynamical behaviors in detail, as shown in Fig. 4, we plot the phase portrait and the corresponding temporal series of the dipole moments for the cases of chaos and periodic self-oscillations extracted from the bifurcation diagrams (Fig. 2). Here, Figs. 4(a) and 4(b) correspond to the case of E = 0.007, where the existence of chaos induces instability, which undergoes different bifurcations leading to a strange attractor. Although the nonperiodic evolution of dipole moments in time domain is quite obvious, we have utilized the quantitative analysis using the method proposed in Ref. [48] to confirm the assessment of chaos. Following the spirit of this method, the Kaplan-Yorke fractal dimension [49] is introduced as

an important quantity to describe chaotic attractor, which is given by $D_{KY} = j + |\Lambda_{j+1}|^{-1} \sum_{i=1}^{j} \Lambda_i$,

where j is the largest integer satisfying $\sum\limits_{i=1}^{j}\Lambda_i\geq 0$ and $\sum\limits_{i=1}^{j+1}\Lambda_i\leq 0$, with $\Lambda_1>\Lambda_2>\Lambda_3>\Lambda_4$. With the phase portraits, the four Lyapunov exponents roughly can be calculated as: $\Lambda_1=0.011074$, $\Lambda_2=0.010881$, $\Lambda_3=-0.024815$, and $\Lambda_4=-0.024839$. Hence, the fractal dimension equals $D_{KY}=2.885>2$, which is quantitatively consistent with the chaotic behavior. While for Figs. 4(c) and 4(d), i.e., for E=0.01, the phase portraits of the dipole moments converge to two limit cycles with periodic self-oscillations in phase plane (see Fig. 4(c)). Combined with the periodic variation of the intensities of the dipole moments shown in Fig. 4(d), we can confirm the state as a periodic self-oscillation state.

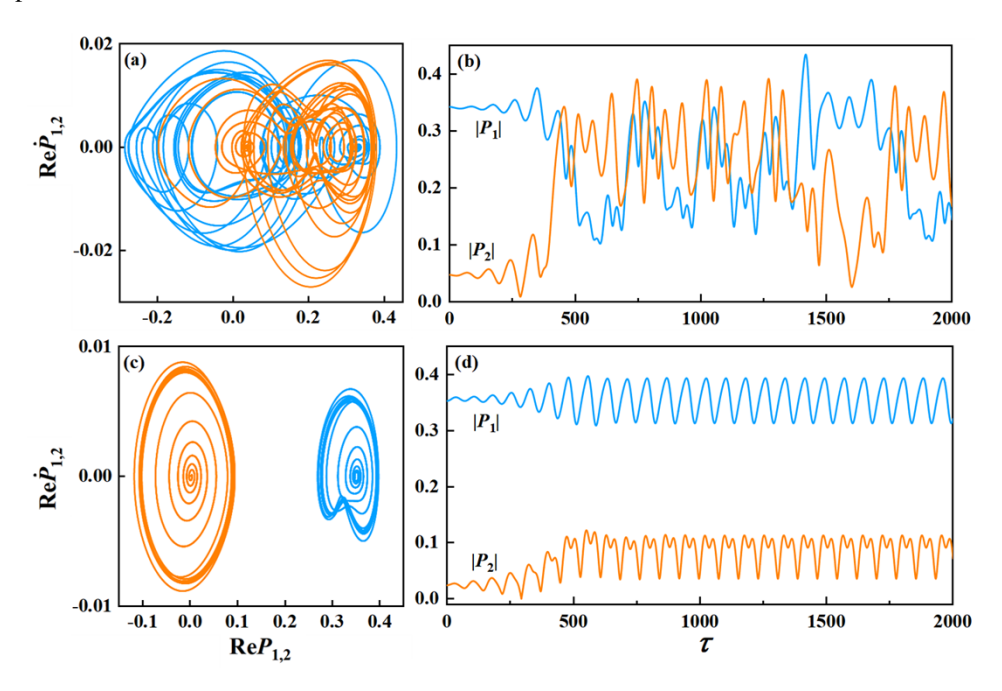


Fig. 4. Phase portraits of dipole moments corresponding to the grey dashed lines in Fig. 2(d) and 2(e) for (a) E = 0.007 and (c) E = 0.01 respectively. Panels (b) and (d) are time evolutions of dipole moments corresponding to the left panels. The blue line represents $|P_1|$ and the orange line is $|P_2|$.

One should notice that the periodic self-oscillations described in Fig. 4(c, d) can coexist with the static multistable states (see the right panels of Fig. 2). In order to realize the free switching among these different states under the same parameters of background field and detuning, we

introduce an extra dimensionless pulse given by

$$E_{ex} = \frac{E_p}{\pi} \left(\arctan \frac{\tau - \tau_0}{\rho} - \arctan \frac{\tau - \tau_0 - \Delta \tau}{\rho} \right), \tag{9}$$

where E_p , τ_0 , $\Delta \tau$ and ρ are the saturation value, starting time, duration time and edge sharpness, respectively. For simplicity, we consider $\rho = 1$, and modulate τ_0 , E_p and $\Delta \tau$ to control the switch of different states. This signal pulse can be treated as a hard excitation whose envelope is in a form of quasi-square function.

As shown in Fig. 5, for the asymmetric nanodimer system with E=0.01, the system starts with an initialized stable static state. When the first pulse with $E_p=0.008$ and $\Delta \tau=150$ is applied, the system can switch into a periodic self-oscillation state with period T=71.4. Due to the asymmetry, energy can be transferred between the dipole moments and two different periods occur simultaneously. After the application of the second pulse with $E_p=0.01$ and $\Delta \tau=100$ at $\tau=3000$, the system can switch into another periodic self-oscillation state with period T=78.3. Accordingly, to further reveal the functionality of this nanodimer acting as an antenna, we present the temporal evolution of the oscillation angle $\theta_{\rm max}$ (the major scattering lobe) in Fig. 5(c). Note that the angular scanning sector of the first self-oscillation state is $\Delta \theta_{\rm max} \simeq 47.8^\circ$, which is much larger than the one of the second self-oscillation state ($\Delta \theta_{\rm max} \simeq 5.3^\circ$). In practical application, combined with the scanning cycles of self-oscillation state, the period 1 can be treated as a quick searching mode with a wide scanning range, while the period 2 can be utilized as a focusing mode with much better directivity for continuous illumination after the detection of a possible

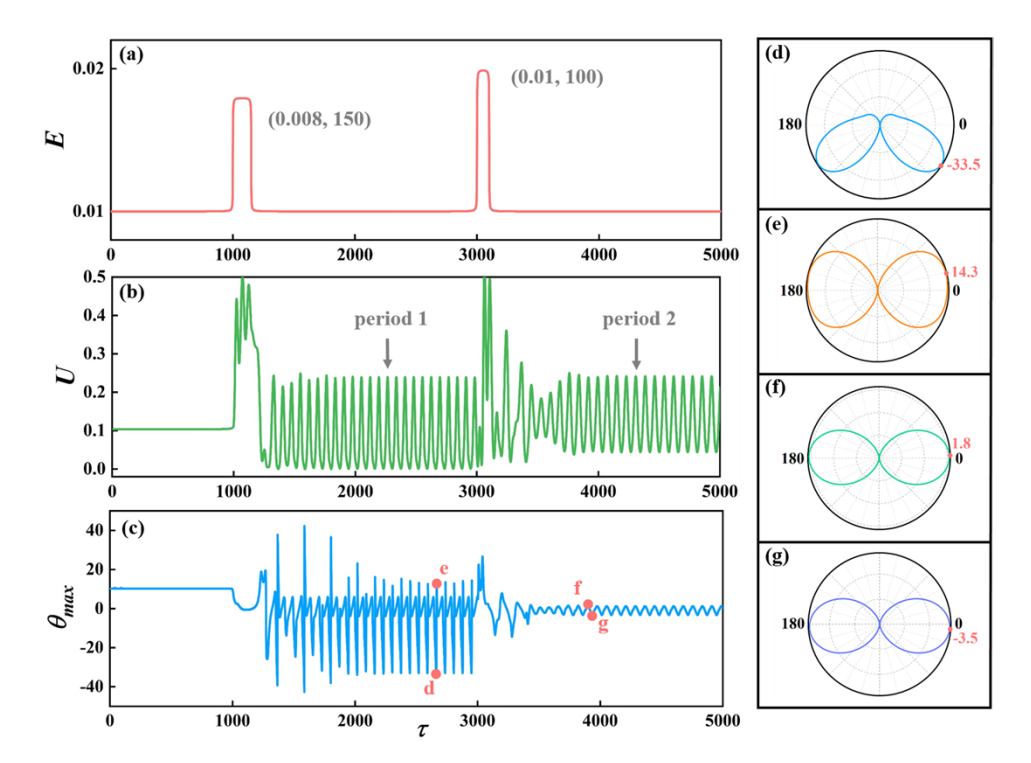


Fig. 5. (a) A rectangular pulse sequence $(E_p, \Delta \tau)$ with original background fields E = 0.01. (b) The corresponding forward scattering intensity. (c) Time evolution of the oscillation angle $\theta_{\rm max}$ (in degrees) corresponding to orientation to the main lobe of the scattering pattern (cut in the *zoy* plane). (d-g) Snapshots of the scattering pattern for the red dots labeled d-g in panel (c). The red numbers show the oscillation angle $\theta_{\rm max}$.

target. In addition, it is well known that the scattering pattern of a conventional antenna can be hardly changed, whereas, the periodic self-oscillations also lead to the ultrafast periodic variation of the scattering pattern (see Fig. 5(d-g)) in this asymmetric nanodimer system. Hence, we can expect that the modulation on the scattering of a nanoantenna via the external excitations should be much more convenient than the other way around [50,51].

Following the spirit of state-switching shown above, we also demonstrate that multistate-switching also can be realized by the application of a sequence of pulses with different parameters under the same background field. We take three stable static states (S1, S2, S3) shown in Fig. 2(f) as an example, and fix the background field at 0.014 in Fig. 6. With the application of a series of pulses whose parameters (E_p , $\Delta \tau$) are: (0.01, 55), (0.005, 50), (0.027, 15), (0.031, 19), (0.008, 50) and (0.048, 14), a tunable tristability switching has been demonstrated. Initially, the output is located in the stable static state S1. When subjected to a sequence of pulses, the output switches sequentially through states S2, S3, S2, S1, S3 and finally returns to S1. After the end of the final pulse, the output remains stable at the state S1 without further change (see Fig. 6(b)). Obviously, such tristability switching has the capability to switch the scattering field between any two of the three states by modulating pulse parameters. In such a way, it is quite convenient for one to realize the expected multistate switching by coding a sequence of pulse signals, which can be promising in optical communication, computing, and quantum information processing [52].

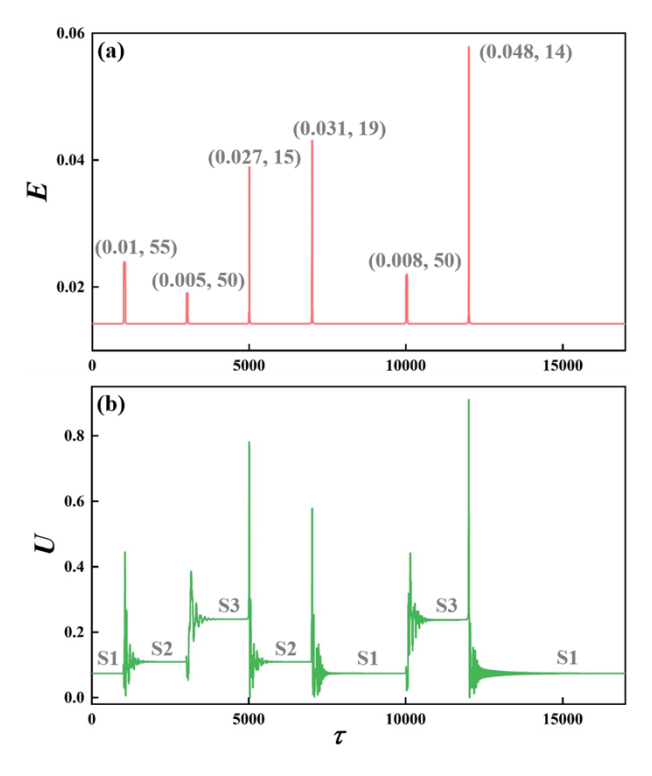


Fig. 6. Multistable states switching under (a) rectangular pulse sequences $(E_p, \Delta \tau)$ with original background fields E = 0.014. Bottom panels (b) show the switch of three stable states marked by stars S1, S2, S3 in Fig. 2.

4. Conclusion

In this work, we perform a comprehensive theoretical analysis of the temporal dynamics for nonlinear nanodimer with asymmetry due to the different graphene layers wrapped on the

two dielectric spheres modulated by the corresponding Fermi energies. Our results reveal the distribution of stable and unstable states in the stationary case, as well as the asymmetry that leads to a greatly enlarged multistable region compared to the symmetry counterpart. We also give the corresponding temporal dynamical behavior, observing stable static states, periodic self-oscillations, period doubling and chaos and carry out a quantitative description on the chaos based on Kaplan-Yorke fractal dimension. In addition, this nanodimer system can operate as a multifunctional nanoantenna for a variety of applications and switching between coexisting states is possible under external excitation pulses. Our work provides an opportunity to manipulate the angular scanning sector and scattering pattern of nanoantenna by applying pulses with different peak values and durations. Meanwhile, optical switching based on multistable states also allows arbitrary switching between two states by a pulse sequence. And these novel phenomena will pave the way for nonlinear nanoantenna and lay the foundation for highly tunable nanophotonic devices.

Funding. National Natural Science Foundation of China (12274314, 12311530763); Natural Science Foundation of Jiangsu Province (BK20221240); Suzhou Basic Research Project (SJC2023003).

Acknowledgments. The authors gratefully acknowledge the financial support from the National Natural Science Foundation of China (Grant Nos. 12274314, 12311530763), Natural Science Foundation of Jiangsu Province (Grant No. BK20221240), and Suzhou Basic Research Project (SJC2023003).

Disclosures. The authors declare no conflicts of interest regarding this article.

Data availability. The data supporting the findings of this study are available from the corresponding author upon reasonable request.

References

- 1. P. A. Franken, A. E. Hill, C. W. Peters, et al., "Generation of optical harmonics," Phys. Rev. Lett. 7(4), 118–119 (1961)
- 2. T. H. Maiman, "Stimulated optical radiation in ruby," Nature 187(4736), 493-494 (1960).
- S. Nakamura, K. Sekiya, S. Matano, et al., "High-speed and on-chip optical switch based on a graphene microheater," ACS Nano 16(2), 2690–2698 (2022).
- 4. J. Yang and X. Zhang, "Optical fiber delivered ultrafast plasmonic optical switch," Adv. Sci. 8(10), 2100280 (2021).
- 5. A. Karnieli, S. Tsesses, G. Bartal, *et al.*, "Emulating spin transport with nonlinear optics, from high-order skyrmions to the topological Hall effect," Nat. Commun. **12**(1), 1092 (2021).
- C. Li, F. Zhou, and K. Yang, "High accuracy optical bistable interferometric fiber sensors," J. Nonlinear Opt. Phys. Mater. 11(02), 125–130 (2002).
- 7. P. Horowitz and W. Hill, *The Art of Electronics*, 3rd ed. (Cambridge University Press, 2015).
- 8. Y. Wang, K. D. Jöns, and Z. Sun, "Integrated photon-pair sources with nonlinear optics," Appl. Phys. Rev. 8(1), 011314 (2021).
- 9. D. Tan, B. Zhang, and J. Qiu, "Ultrafast laser direct writing in glass: Thermal accumulation engineering and applications," Laser Photonics Rev. 15(9), 2000455 (2021).
- C. Wang, D. Gao, and L. Gao, "Detecting nonlocality by second-harmonic generation from a graphene-wrapped nanoparticle," Opt. Express 30(8), 12722 (2022).
- A. Husakou and J. Herrmann, "Steplike transmission of light through a metal-dielectric multilayer structure due to an intensity-dependent sign of the effective dielectric constant," Phys. Rev. Lett. 99(12), 127402 (2007).
- 12. C. R. Gubbin and S. De Liberato, "Theory of four-wave-mixing in phonon polaritons," ACS Photonics 5(2), 284–288 (2018)
- 13. L. L. Bonilla, M. Alvaro, and M. Carretero, "Chaos-based true random number generators," J. Math. Ind. 7(1), 1
- B. Karakaya, A. Gülten, and M. Frasca, "A true random bit generator based on a memristive chaotic circuit: Analysis, design and FPGA implementation," Chaos, Solitons Fractals 119, 143–149 (2019).
- A. Buscarino, L. Fortuna, M. Frasca, et al., "Memristive chaotic circuits based on cellular nonlinear networks," Int. J. Bifurc. Chaos 22(03), 1250070 (2012).
- S. Bittner, S. Guazzotti, Y. Zeng, et al., "Suppressing spatiotemporal lasing instabilities with wave-chaotic microcavities," Science 361(6408), 1225–1231 (2018).
- N. Lapshina, R. Noskov, and Y. Kivshar, "Nanoradar based on nonlinear dimer nanoantenna," Opt. Lett. 37(18), 3921 (2012).
- N. S. Lapshina, R. E. Noskov, and Y. S. Kivshar, "Nonlinear nanoantenna with self-tunable scattering pattern," JETP Lett. 96(12), 759–764 (2013).
- Z. Ziani, G. Lévêque, S. Coulibaly, et al., "Investigating route to chaos in nonlinear plasmonic dimer," Ann. Phys. 532(10), 2000240 (2020).

- P. Ma, L. Gao, P. Ginzburg, et al., "Ultrafast cryptography with indefinitely switchable optical nanoantennas," Light Sci. Appl. 7(1), 77 (2018).
- R. E. Noskov, A. E. Krasnok, and Y. S. Kivshar, "Nonlinear metal-dielectric nanoantennas for light switching and routing," New J. Phys. 14(9), 093005 (2012).
- P. Ma, D. Gao, Y. Ni, et al., "Enhancement of Optical Nonlinearity by Core-Shell Bimetallic Nanostructures," Plasmonics 11(1), 183–187 (2016).
- R. E. Noskov, P. A. Belov, and Y. S. Kivshar, "Subwavelength modulational instability and plasmon oscillons in nanoparticle arrays," Phys. Rev. Lett. 108(9), 093901 (2012).
- R. E. Noskov, D. A. Smirnova, and Y. S. Kivshar, "Subwavelength solitons and Faraday waves in two-dimensional lattices of metal nanoparticles," Opt. Lett. 38(14), 2554 (2013).
- R. S. Savelev, A. V. Yulin, A. E. Krasnok, et al., "Solitary waves in chains of high-index dielectric nanoparticles," ACS Photonics 3(10), 1869–1876 (2016).
- R. Noskov, P. Belov, and Y. Kivshar, "Oscillons, solitons and domain walls in arrays of nonlinear plasmonic nanoparticles," Sci. Rep. 2(1), 873 (2012).
- Y. Huang and L. Gao, "Broadened region for robust optical bistability in a nonlocal core and Kerr shell nanoparticle," Opt. Lett. 43(12), 2836 (2018).
- Y. Huang, L. Gao, P. Ma, et al., "Nonlinear chaotic dynamics in nonlocal plasmonic core-shell nanoparticle dimer," Opt. Express 31(12), 19646 (2023).
- B. I. Afinogenov, V. O. Bessonov, A. A. Nikulin, et al., "Observation of hybrid state of Tamm and surface plasmon-polaritons in one-dimensional photonic crystals," Appl. Phys. Lett. 103(6), 061112 (2013).
- 30. P. Ma, L. Gao, P. Ginzburg, *et al.*, "Nonlinear nanophotonic circuitry: Tristable and astable multivibrators and chaos generator," Laser Photonics Rev. **14**(3), 1900304 (2020).
- Y. Huang, A. E. Miroshnichenko, and L. Gao, "Low-threshold optical bistability of graphene-wrapped dielectric composite," Sci. Rep. 6(1), 23354 (2016).
- 32. H. Chen and Y. Huang, "Tunable optical force on nonlinear graphene-wrapped nanoparticles," Phys. Lett. A **384**(28), 126733 (2020).
- 33. K. Zhang, Y. Huang, A. E. Miroshnichenko, *et al.*, "Tunable optical bistability and tristability in nonlinear graphene-wrapped nanospheres," J. Phys. Chem. C **121**(21), 11804–11810 (2017).
- T. Naseri and M. Balaei, "Enhanced nonlinear optical response of core-shell graphene-wrapped spherical nanoparticles," J. Opt. Soc. Am. B 35(9), 2278 (2018).
- 35. X. Jiang, Y. Huang, P. Ma, et al., "Temporal dynamics of an asymmetrical dielectric nanodimer wrapped with graphene," Photonics 10(8), 914 (2023).
- 36. Y. Huang, P. Ma, and Y. M. Wu, "Abnormal fano profile in graphene-wrapped dielectric particle dimer," Photonics 7(4), 124 (2020).
- J. S. Lee, K. H. You, and C. B. Park, "Highly photoactive, low bandgap TiO 2 nanoparticles wrapped by graphene," Adv. Mater. 24(8), 1084–1088 (2012).
- 38. P. Wu, H. Wang, Y. Tang, *et al.*, "Three-dimensional interconnected network of graphene-wrapped porous silicon spheres: In situ magnesiothermic-reduction synthesis and enhanced lithium-storage capabilities," ACS Appl. Mater. Interfaces **6**(5), 3546–3552 (2014).
- 39. H. H. Li, "Refractive index of alkaline earth halides and its wavelength and temperature derivatives," J. Phys. Chem. Ref. Data 9(1), 161–290 (1980).
- T. Christensen, W. Yan, A.-P. Jauho, et al., "Kerr nonlinearity and plasmonic bistability in graphene nanoribbons," Phys. Rev. B 92(12), 121407 (2015).
- 41. T. Naseri, N. Daneshfar, M. Moradi-Dangi, *et al.*, "Terahertz optical bistability of graphene-coated cylindrical core–shell nanoparticles," J. Theor. Appl. Phys. **12**(4), 257–263 (2018).
- I. Olivares, R. Rojas, and F. Claro, "Surface modes of a pair of unequal spheres," Phys. Rev. B 35(5), 2453–2455 (1987).
- W. Yu, P. Ma, H. Sun, et al., "Optical tristability and ultrafast Fano switching in nonlinear magnetoplasmonic nanoparticles," Phys. Rev. B 97(7), 075436 (2018).
- 44. Z. Ziani, G. Lévêque, A. Akjouj, et al., "Characterization of spatiotemporal chaos in arrays of nonlinear plasmonic nanoparticles," Phys. Rev. B 100(16), 165423 (2019).
- D. J. Bergman, O. Levy, and D. Stroud, "Theory of optical bistability in a weakly nonlinear composite medium," Phys. Rev. B 49(1), 129–134 (1994).
- 46. L. Gao, "Optical bistability in composite media with nonlinear coated inclusions," Phys. Lett. A **318**(1-2), 119–125 (2003)
- 47. T. Shegai, S. Chen, V. D. Miljković, *et al.*, "A bimetallic nanoantenna for directional colour routing," Nat. Commun. **2**(1), 481 (2011).
- 48. K. Ramasubramanian and M. S. Sriram, "A comparative study of computation of Lyapunov spectra with different algorithms," Phys. Nonlinear Phenom. **139**(1-2), 72–86 (2000).
- 49. J. L. Kaplan and J. A. Yorke, Functional Differential Equations and Approximation of Fixed Points (Springer, 1979).
- 50. M. Abb, P. Albella, J. Aizpurua, *et al.*, "All-optical control of a single plasmonic nanoantenna–ITO hybrid," Nano Lett. **11**(6), 2457–2463 (2011).

- 51. J. Berthelot, A. Bouhelier, C. Huang, *et al.*, "Tuning of an optical dimer nanoantenna by electrically controlling its load impedance," Nano Lett. **9**(11), 3914–3921 (2009).
- 52. J. Jiang, C. Strother, K. Johnson, *et al.*, "Comparison of blood velocity measurements between ultrasound Doppler and accelerated phase-contrast MR angiography in small arteries with disturbed flow," Phys. Med. Biol. **56**(6), 1755–1773 (2011).